IEEE Access
Multidisciplinary | Rapid Review | Open Access Journal

Received September 2, 2021, accepted September 21, 2021, date of publication September 24, 2021,
date of current version October 5, 2021.

Digital Object Identifier 10.1109/ACCESS.2021.3115512

Series DC Arc Fault Detection Using Machine Learning Algorithms

HOANG-LONG DANG[1], JAECHANG KIM[1], SANGSHIN KWAK[1], (Member, IEEE), AND SEUNGDEOG CHOI[2], (Senior Member, IEEE)

[1]School of Electrical and Electronics Engineering, Chung-Ang University, Seoul 06974, South Korea
[2]Department of Electrical and Computer Engineering, Mississippi State University, Starkville, MS 39762, USA

Corresponding authors: Sangshin Kwak (sskwak@cau.ac.kr) and Seungdeog Choi (seungdeog@ece.msstate.edu)

This work was supported in part by the National Research Foundation of Korea (NRF) grant funded by the Korea government (MSIT) (2020R1A2C1013413), and in part by the Technology Development Program to Solve Climate Changes through the National Research Foundation of Korea (NRF) funded by the Ministry of Science, ICT (2021M1A2A2060313).

ABSTRACT The wide variety of arc faults induced by different load types renders residential series arc fault detection complicated and challenging. Series dc arc faults could cause fire accidents and adversely affect power systems if not promptly detected. However, in practical power systems, they are difficult to detect because of a low arc current, absence of a zero-crossing period, and various abnormal behavior based on different types of power loads and controllers. In particular, conventional protection fuses may not be activated when they occur. Undetected arc faults could cause false operation of power systems and potentially lead to damage to property and human casualties. Therefore, it is imperative to develop a detection system for series arc faults in DC systems for the reliable and efficient operation of such systems. In this study, several typical loads, especially nonlinear and complex loads such as power electronic loads, were chosen and analyzed, and five time-domain parameters of the current—average value, median value, variance value, RMS value, and distance of the maximum and minimum values—were chosen for arc fault detection. Various machine learning algorithms were used for arc fault detection and their detection accuracies were compared.

INDEX TERMS Arc fault detection, artificial intelligence, DC arc fault, machine learning, series arc.

I. INTRODUCTION

Recently, renewable energy has drawn attention owing to its advantages, such as green techniques and low carbon dioxide emission, and studies have been conducted on integrating them into existing power networks [1]–[4]. Although DC power systems are becoming an essential part of renewable energy systems, DC power systems have some inherent challenges. In particular, the occurrence of arc faults is one of the most critical problems. Arc faults could lead to high temperatures, intense light, and noise. Hence, they could potentially result in surrounding materials catching fire and thereby cause economic loss [5]. There are two main types of arc faults in DC power systems: series and parallel arc faults [6], [7]. A series arc fault is generated by the disconnection of a conductor in transmission power lines, whereas a parallel arc fault results from the insulation breakdown between two or more parallel lines because of an external force or heat. For the safety of DC systems, it is vital to detect arc faults promptly; therefore, arc fault detection techniques are essential. Generally, parallel arc faults exciting different current flows, and the rapid increase in the arc fault current can be eliminated by using devices such as fuses. Series arc faults act like an additional impedance in the system and cause the arc fault current to decrease. Consequently, conventional protection devices cannot be activated [8]. If not detected and eliminated promptly, series arc faults could affect the system's related circuits, damage the power supply sources and system controller, and even cause explosions. In DC networks, most of the components are connected through electronic circuits or converters, and the electromagnetic distortion noise produced by electronic converters renders arc fault detection more challenging. Therefore, several approaches to detect series arc faults and numerous studies have been conducted to analyze the characteristics of series arc faults.

There are several types of research on arc fault detection. Mathematical models of arc faults have been

The associate editor coordinating the review of this manuscript and approving it for publication was Inam Nutkani.

developed using experimental data [9]–[13]. However, the models do not comprehensively describe the external characteristics of the arc and are suitable for theoretical investigation and studies. Furthermore, arc fault detection methods based on the characteristics of arc faults, such as intense light, high temperature, considerable distortion noise, and high electromagnetic radiation, have been developed in [14]–[20]. However, their major drawback is their incapability to locate the positions of arc faults correctly [21]. With the advancement of information technology, artificial intelligence (AI) methods have become popular and offer potential techniques in fault diagnosis in various areas such as high impedance fault detection in medium voltage networks [22], failure detection in electrical machines [23], and track circuit fault detection in railway systems [24]. Several recent studies have achieved promising results for DC series arc fault detection with AI-based methods, such as the combined use of a support vector machine (SVM) and wavelet packet decomposition for series arc fault detection [25], the use of a hidden Markov model (HMM) for obtaining the maximum likelihood of series arc faults for correctly detecting faults [26], and the use of a cascaded fuzzy logic system in a photovoltaic system for series arc fault detection [27]. Numerous features such as current variations and high-frequency energy are extracted, trained for series arc detection based on weighted least squares SVM algorithms [28]. Furthermore, an attractor matrix was constructed from current signals and feature extraction based on singular value decomposition was proposed in [29], sparse coding features and a neural network were combined for arc fault detection in [30], and the combination of domain adaptation and a deep convolutional generative adversarial network was presented in [31]. A report in [32] presents a comparison between various learning techniques in DC photovoltaic system. Generally, these studies focus only on one control technique or one particular switching frequency for specific loads. On the other hand, the performances of AI algorithms are greatly affected by the operating conditions. The effects of different operation conditions on arc detection are still an open question for the researcher. There is a need for an overview study with various load types, control techniques, input features, switching frequencies.

In this paper, five input features and eight AI algorithms have been executed and compared, the types of input parameters such as average value, median value, variance value, RMS value, and the difference between the maximum and minimum value [33]. Comparing the performance according to the combination of AI algorithms and five input features of different load types is presented. This paper is organized as follows. Section 2 describes the experimental setup and how the current characteristics in each of the normal and arcing parts change in the time domain when a series arc occurs. Section 3 details the AI algorithms used for arc fault detection and feature analysis techniques used for series arc detection in this study. Section 4 presents detection results obtained using the eight AI algorithms and five input features in enclosed and unenclosed cases when a series arc fault occurred for different load types and operating frequencies. Finally, the conclusion of the arc fault detection according to AI algorithms is presented in Section 5.

II. SERIES DC ARC CHARACTERISTICS

Figure 1 shows a circuit diagram for obtaining series arc data. To obtain the data, we designed the arc-generating circuit regarding UL1699B [34]. Separating the arc rods generated an arc, and an oscilloscope was used to save the currents flowing through the rods before and after arcing. MATLAB was used to analyze the arc currents. The arc generation experiment setup comprised a DC power supply, arc generator, and loads. An N8741A DC power supply (Keysight Technologies, USA) was employed in the experiment. Table 1 presents the specifications of loads used in the experiment. The three- and single-phase inverters were constructed using an insulated-gate bipolar transistor module (SKM50GB123D, SEMIKRON, Germany). The switching frequency of the model predictive control (MPC) technique was variable. In this study, the switching frequency was the average switching frequency obtained from the number of times the switch was turned on and off in a specific interval. The current amplitude was the arc current magnitude before arcing. In the case of inverter loads, the arc current before and after arcing was the inverter's input current [35].

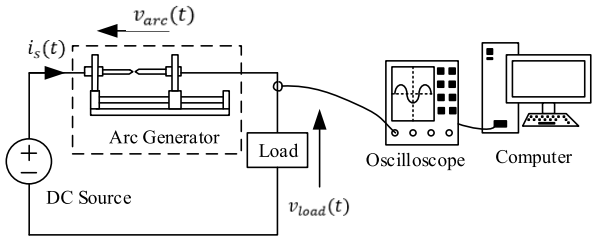

FIGURE 1. DC series arc schematic.

As shown in Figure 1, a DC voltage was supplied to the load. Subsequently, the step motor, which was connected to the arc rods, was switched on to separate the arc rods. The data were sampled by an oscilloscope (Tektronix MSO3054, USA) at 250 kHz sampling frequency. Tektronix TCP312 (Tektronix, OR, USA) was used as the current probe to measure the arc current. The recorded data were split into smaller data sets of 2 ms for training and testing the AI algorithms. Figure 2 presents the structures of the three-phase and single-phase inverters that were used as loads in this study. These inverters converted DC signals into AC signals, and during their operation, only one switch was connected in each phase leg at any given instant. This led to eight and four switching vectors for the operation of the three-and single-phase inverters, respectively. This study employed space vector modulation (SVPWM), MPC, and sinusoidal pulse width modulation (SPWM) to control the three-phase and single-phase inverters. SVPWM is

TABLE 1. Specifications of loads used in the experiment.

Load types	Control techniques	Switching frequencies [kHz]	Current amplitudes [A]
Three-phase inverter	Space vector modulation	5, 10, 15, 20	3, 4, 5, 6, 7, 8
	Model predictive control	5, 10, 15, 20	5, 8
Single-phase inverter	Sinusoidal pulse width modulation	5, 10, 15, 20	5
Resistor	N/A	N/A	5, 8

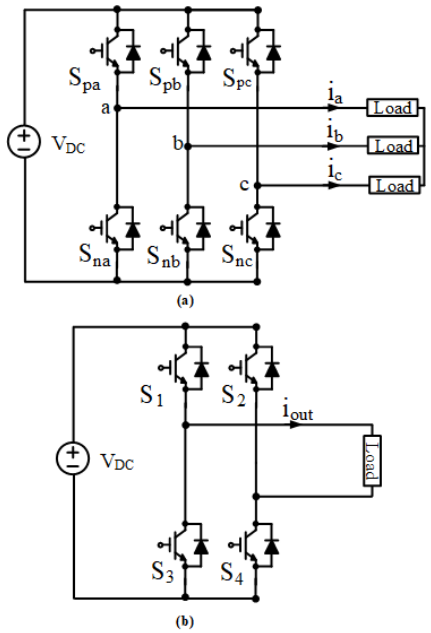

FIGURE 2. Converter structures: (a) three-phase inverter and (b) single-phase inverter.

a modulation technique for the control of pulse width modulation. The objective was to use a given DC voltage and control six switches to emulate three-phase sinusoidal waveforms whose frequency and amplitude was adjustable. MPC is an advanced method of process control while satisfying one or several constraints. It involves dynamic models of the circuit. SPWM is a typical PWM technique. The sinusoidal AC voltage reference was compared with the high-frequency triangular carrier wave to determine the switching state for each leg in the inverter. Different control techniques were used to compare the performance of arc detection for various conditions for obtaining an overview of the effectiveness of

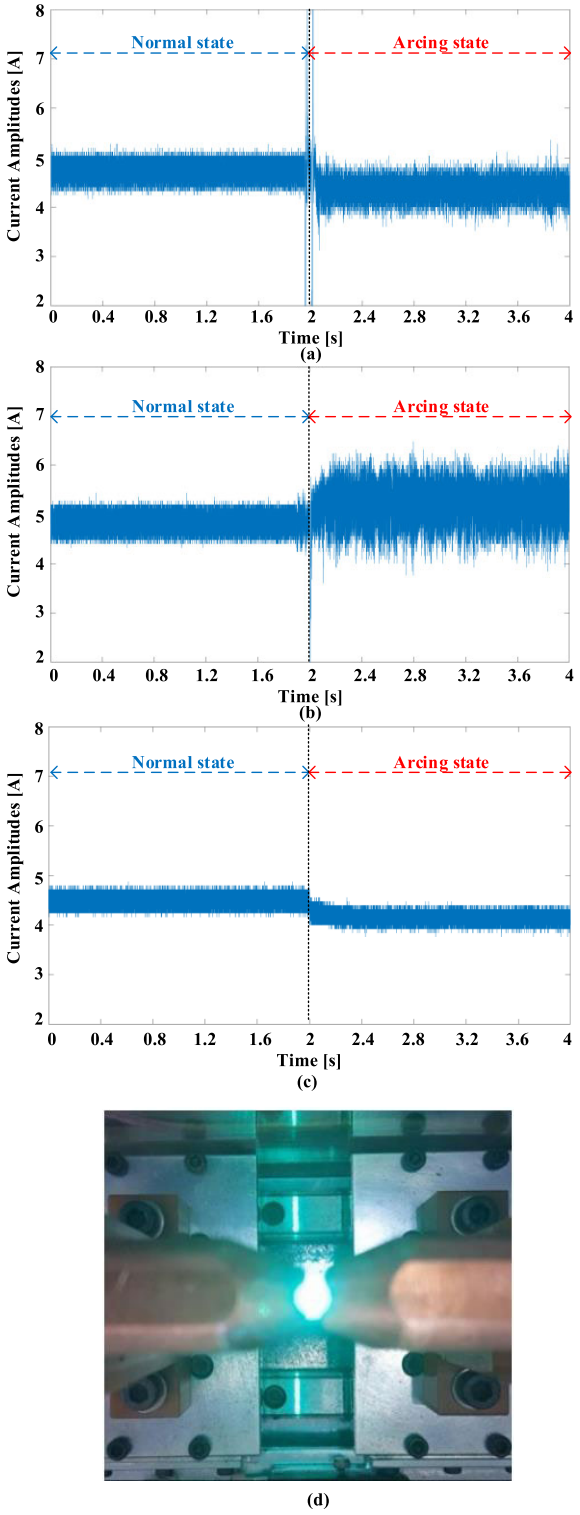

FIGURE 3. Current waveforms for different loads from the normal state to the arcing state. (a) Three-phase inverter load with SVPWM at 5 kHz, (b) three-phase inverter load with MPC at 5 kHz, (c) resistor load, and (d) arc generation.

the different artificial learning algorithms. Figure 3 shows the normal and arcing state waveforms for different loads. For all the loads, the shapes of the waveforms before arcing

were similar. When an arc was generated, the waveforms showed many abnormal behaviors, such as the addition of harmonic components to the load current, the distortion of the load current waveform, and a decrease in the current amplitude. The large amplitude spikes during the initial arcing state in the current were caused by electrical sparks. The magnitude of electrical sparks could be large or small, depending on the type of load. The aforementioned abnormal behaviors could be potentially used for arc fault detection.

III. ARTIFICIAL INTELLIGENCE ALGORITHMS

A. STRUCTURES OF ARTIFICIAL INTELLIGENCE ALGORITHMS

1) SUPPORT VECTOR MACHINE

The SVM is based on a framework called Vapnik–Chervonenkis (VC) theory. Then, Boser and colleagues presented an algorithm that maximizes the margin between training data [36]. The SVM aims to find the best hyperplane that can separate data from two different classes with the maximum margin, and it can perform linear or nonlinear classifications based on the features of the data. The best classifier is the SVM, with the hyperplane has the largest margin.

2) K-NEAREST NEIGHBOR

Evelyn Fix and Joseph Hodges proposed the K-nearest neighbors (KNN) algorithm. The basic concept of the classification algorithm is that if an object has K most similar neighbors in its vicinity and if most of them are located in a specific class, the object is also located in that class [37].

3) RANDOM FOREST

Random forest (RF) is an ensemble learning method for classification, regression, and other tasks, and it constructs multiple decision trees during training time and at the output [38]. The forests pull together the decision tree algorithms, take the teamwork of many trees, and improve the performance of a single random tree.

4) Naïve BAYES

Naive Bayes (NB) is the simplest form of Bayesian network classifiers [39]. Naïve Bayes classifiers require several parameters to be linear in the number of variables (features/predictors) in a learning problem. Naive Bayes is a typical method for constructing classifiers: assigning class labels to objects represented as vectors of feature values.

5) DECISION TREE

One of the most popular classification models is the decision tree (DT) model. DTs are popular because they are practical and easy to understand. Furthermore, rules can be easily extracted from DTs [40]. Classification trees perform the classification function by using a top-down process that divides the input training data into smaller branches until a branch that shows the most appropriate label is reached. The DT structure consists of a root, several nodes, branches, and leaves (also known as decision points), which are class labels.

6) DEEP NEURAL NETWORK

The deep neural network (DNN) structure consists of n parameters as inputs, and these inputs are passed through a network composed of N layers to obtain the final results. This process is repeated N times. The state of the first layer was as follows:

$$\boldsymbol{h}_1 = f_1\left(\boldsymbol{W}_1^T \boldsymbol{X} + \boldsymbol{b}_1\right) \tag{1}$$

$\boldsymbol{X}$ is the input parameter, $\boldsymbol{W}_1^T$ is the weight of the first layer, and $\boldsymbol{b}_1$ is the bias in the first layer. $\boldsymbol{h}_1$ is the output of the first layer, which is transferred to the second layer. The primary learning method of multiple artificial neural networks is to evaluate one epoch and then use the error to update the weight and the bias value to reduce each layer's error. This method is called error backpropagation. There are different types of neural networks, but all of them consist of the same components: neurons, weights, biases, and functions. These components function similarly to the human brain and can be trained like any other machine learning algorithm. In this layer, the neurons are connected fully with the neurons of the previous layer. It has the simplest structure and plays an important role in connecting all neurons located in the preceding and following layers. If all neurons of all layers are fully connected (FC), the neural network is called DNN.

7) LONG SHORT-TERM MEMORY

Long short-term memory (LSTM) belongs to the recurrent neural network (RNN) algorithm. An LSTM unit has three gates: a forget gate, an input gate, and an output gate. These gate structures can achieve efficient feedback of adequate information through selective forgetting and memory mechanisms, thereby making the network achieve the approximation of complex time-varying nonlinear functions better. In LSTM, the long-term memory and the short-term memory are controlled separately. Equation (2) shows the output of each LSTM neuron.

$$y_t = (\sigma\,(h_{t-1}x_t + W_0 h_{t-1} + C_t C_{t-1} + b_o))\,tanh\,(c_t) \tag{2}$$

where σ is a variable that determines how much the weight and bias values are changed for the data received in one iteration as the learning rate. h_{t-1} and h_t are the short-term memory states at the previous moment and at present, respectively. C_{t-1} and C_t are the long-term memory states at the previous moment and at present, respectively. W_0 and b_o are the current weight and bias of current LSTM cell, respectively. x_t represents the input data, which come from another LSTM cell. y_t represents the output data, which is sent to another LSTM cell.

8) GATED RECURRENT UNIT

Gated recurrent unit (GRU) is also an RNN algorithm. Unlike LSTM, long-term memory and short-term memory are

combined in GRU. There are two main gates in GRU, namely, update and reset gates. The function of the update gate is to control previous state information flows into the current state. The role of the reset gate is to control the ignored degree of status information at the last moment. Equation (3) shows the output of each GRU neuron.

$$h_t = z_t \hat{h}_t + (1 - z_t)\, h_{t-1} \tag{3}$$

where h_{t-1} and h_t are the memory states at the previous and present time, respectively. z_t, $\hat{h}_t$ are the update gate vector and candidate activation vector, and x_t is the current input.

Table 2 shows the layer structures of three deep learning techniques (DNN, LSTM, and GRU). DNN had four FC layers, and the number of neurons in layers 1, 2, 3, and 4 were 4, 5, 5, and 2, respectively. LSTM and GRU had five layers, and the number of neurons in layers 1, 2, 3, 4, and 5 were 16, 16, 8, 8, and 2, respectively. The second and fourth layers of LSTM are different from those of GRU. The properties of hidden layers such as the number of layers and neurons are chosen by the trial and error method. The present structures showed the best performance among various structures. However, there may be other suitable layer configurations.

TABLE 2. Structures of neural networks used for DC series arc fault detection.

Networks	Layer 1	Layer 2	Layer 3	Layer 4	Layer 5
DNN	FC/4	FC/5	FC/5	FC/2	N/A
LSTM	FC/16	LSTM/ 16	FC/8	LSTM/8	FC/2
GRU	FC/16	GRU/16	FC/8	GRU/8	FC/2

B. INPUT PARAMETERS

A feature is a critical part of machine learning implementation. A group of features can illustrate the original input data, but not wholly represent the original data. Thus, the more the number of features used, the ML algorithm is more effective. However, if the number of features is too high, the classification performance can be degraded or overfitting can occur. Several techniques can obtain features from the input data, such as fast Fourier transform and wavelet transformation. However, these features pertain to the frequency domain, and their extraction requires high sampling frequency and computational cost. In practical systems, these drawbacks could delay the processing time and affect accuracy when arc faults occur. By contrast, features in the time domain can be extracted with a low sampling frequency, which offers a fast computation effort. Therefore, time-domain features were utilized for arc fault detection in this study. The data were sampled at 250 kHz sampling frequency. Then, the recorded data were split into smaller data sets of 2 ms for training and testing the AI algorithms. For each data set, the signal is processed to obtain one feature set of five values for average, median, variance, rms, and distance between the maximum and minimum currents. After that, these feature sets were used as input for eight learning techniques to detect series DC arc faults.

IV. SERIES DC ARC FAULT DETECTION USING ARTIFICIAL INTELLIGENCE ALGORITHMS

Arc detection using AI algorithms can be divided into two types. The first type is when the test data of a category has already been trained, and the second type is when the test data of a category has not been trained. These cases are referred to as enclosed types and unenclosed types, respectively. Figure 4 shows the structure of a confusion matrix. CN and CA are the correctly predicted data sets for the normal and arcing states, respectively. MD indicates "missing detection," and it refers to the arcing state data set being predicted as the normal state. FD is "false detection," and it refers to the normal state data set being predicted as the arcing state. The numerals 0 and 1 signify the normal state and arcing state, respectively.

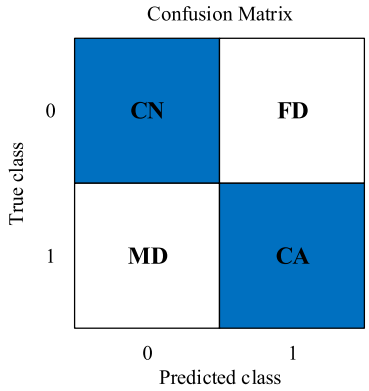

FIGURE 4. Structure of confusion matrix.

To evaluate the performance of the AI algorithms, we used the following metrics. The dummy detection rate is the ratio between the number of normal state data sets predicted as the arcing state and the total number of normal state data sets. It is expressed as

$$\%\ of\ Dummy\ Det. = \frac{\#\ of\ normal\ data\ sets\ predicted\ as\ arcing\ state}{total\ \#\ of\ normal\ data\ sets}. \tag{4}$$

The missing detection rate is the ratio between the number of arcing state data sets predicted as the normal state and the total number of arcing state data sets. It is expressed as

$$\%\ of\ Missing\ Det. = \frac{\#\ of\ arcing\ data\ sets\ predicted\ as\ normal\ state}{total\ \#\ of\ arcing\ data\ sets}. \tag{5}$$

The accuracy detection rate is the ratio of the number of correctly predicted data sets to the total number of test data sets. It is expressed as

$$\%\ of\ Total\ Acc. = \frac{\#\ of\ correctly\ predicted\ data\ sets}{total\ \#\ of\ test\ data\ sets}. \tag{6}$$

The best detection technique is the technique with the lowest dummy and lowest missing detection rates or highest accuracy. The distribution of training and test data is shown in Figure 5. The data were divided into three groups. Group 1 consisted of current data of the three-phase inverter load with SVPWM control at current amplitudes of 3, 5, and 8 A, and the switching frequencies varied from 5 to 20 kHz. Group 2 consisted of current data of the resistor load, the three-phase inverter load with MPC, and the single-phase inverter load with PWM control. The current amplitudes were 5 and 8 A, and the switching frequencies varied from 5 to 20 kHz. Group 3 consisted of current data of the three-phase inverter load with SVPWM control. The current amplitudes were 4, 6, and 7 A, and the switching frequencies were 15 and 20 kHz. This group was employed as a neutral group, and it was not used for training but only for testing. Figure 5(a) shows the distribution of training data and test data for series DC arc detection for the enclosed type; 22,800 data sets of the normal state and arc state were entered into the training data, and 18,400 data sets were entered into the test data. The test data were excluded from the training data. Figure 5(b) shows the distribution of training data and test data for series DC arc detection for the unenclosed type. There were two cases in this type, and for simplicity, they were named unenclosed type 1 and unenclosed type 2. In unenclosed type 1, the data in group 1 were trained, and the data in groups 2 and 3 were used for the test. In unenclosed type 2, the data in group 2 were used for training, and those in groups 1 and 3 were used for the test. The ratio between the normal and arcing data sets in all the training and test processes was 1:1.

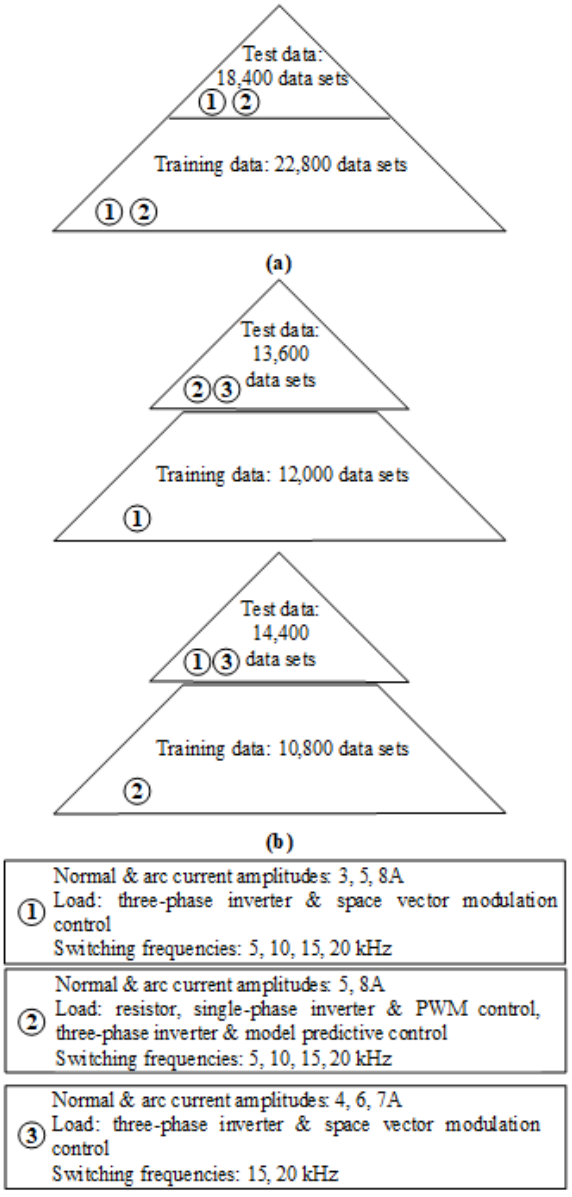

FIGURE 5. Contribution of training and test data. (a) Enclosed type and (b) unenclosed type.

A. ENCLOSED TYPES

Figure 6 shows dummy detection rates for the enclosed type when different DC current amplitudes and various loads were employed. In the case of three-phase inverter load with SVPWM, the dummy detection rates of the five machine learning techniques were always lower than those of the three deep learning techniques in all frequency ranges at 3 A. At 5 A, KNN, RF, NB, DT, and GRU techniques were lower than the remaining three learning techniques in all frequency ranges. At 8 A and three-phase inverter load with SVPWM, KNN, RF, NB, DT were lower than the other techniques in frequency ranges 5 to 15 kHz and vice versa in 20 kHz switching frequency. In the case of three-phase inverter load with MPC, all techniques showed similar performance except DNN for both 5 and 8 A current amplitudes in all frequency ranges. A similar trend was observed for the case of single-phase inverter and resistor load. Generally, KNN, RF, NB, and DT showed high performance compared with SVM and three deep learning techniques. Figure 7 shows missing detection rates for the enclosed type when different DC current amplitudes and various loads were employed. In the case of three-phase inverter load with SVPWM, the missing detection rates of KNN, RF, NB, and DT were lower than that of other techniques in all frequency ranges except NB at 3 A. In the case of three-phase inverter load with MPC, all techniques showed similar performance except SVM for both 5 and 8 A current amplitudes in all frequency ranges. A similar trend was also observed for the case of single-phase inverter and resistor load.

Figure 8 shows accuracy detection rates for the enclosed type when different DC current amplitudes and various loads were employed. In the case of three-phase inverter load with SVPWM at 3 A, DT showed the highest accuracy and GRU showed the lowest accuracy at 5 and 15 kHz switching frequencies. At 10 kHz, NB showed the highest accuracy and GRU showed the lowest accuracy. At 20 kHz, DT showed the highest accuracy and NB showed the lowest accuracy. Among the five machine learning techniques, DT showed the best performance and SVM had the lowest accuracy. Among the three deep learning techniques, DNN showed the best

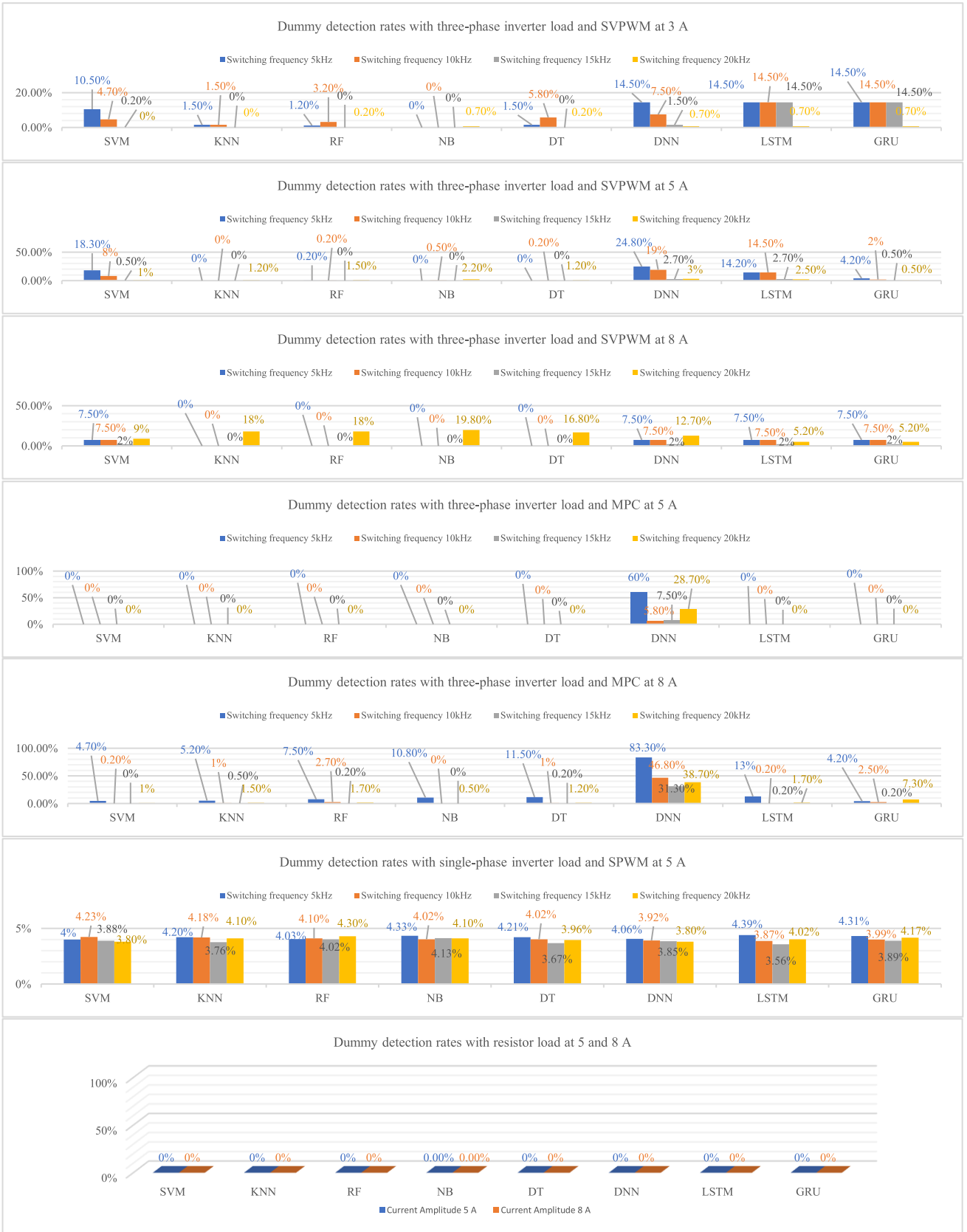

FIGURE 6. **Dummy detection rates for the enclosed type in different conditions.**

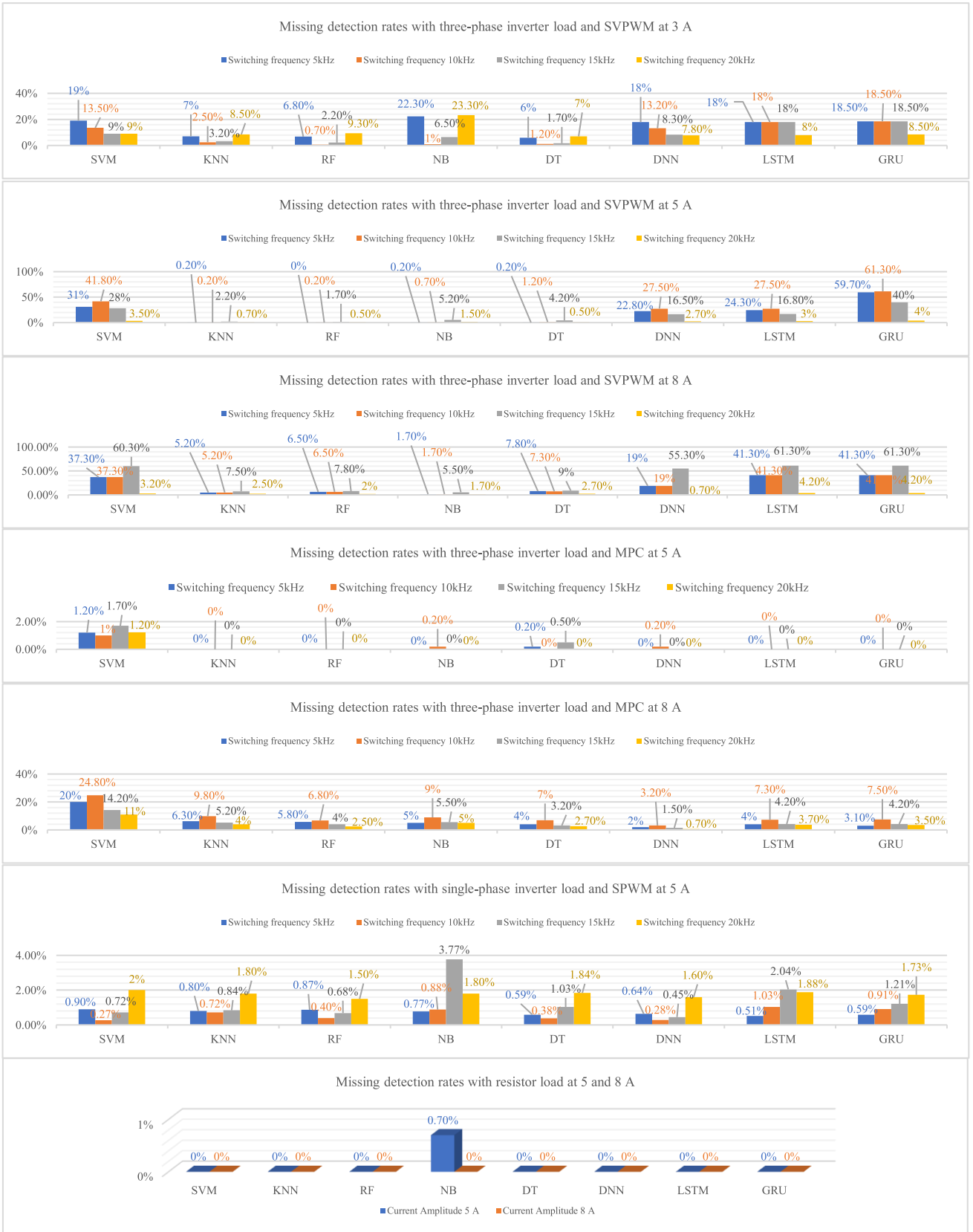

FIGURE 7. Missing detection rates for the enclosed type in different conditions.

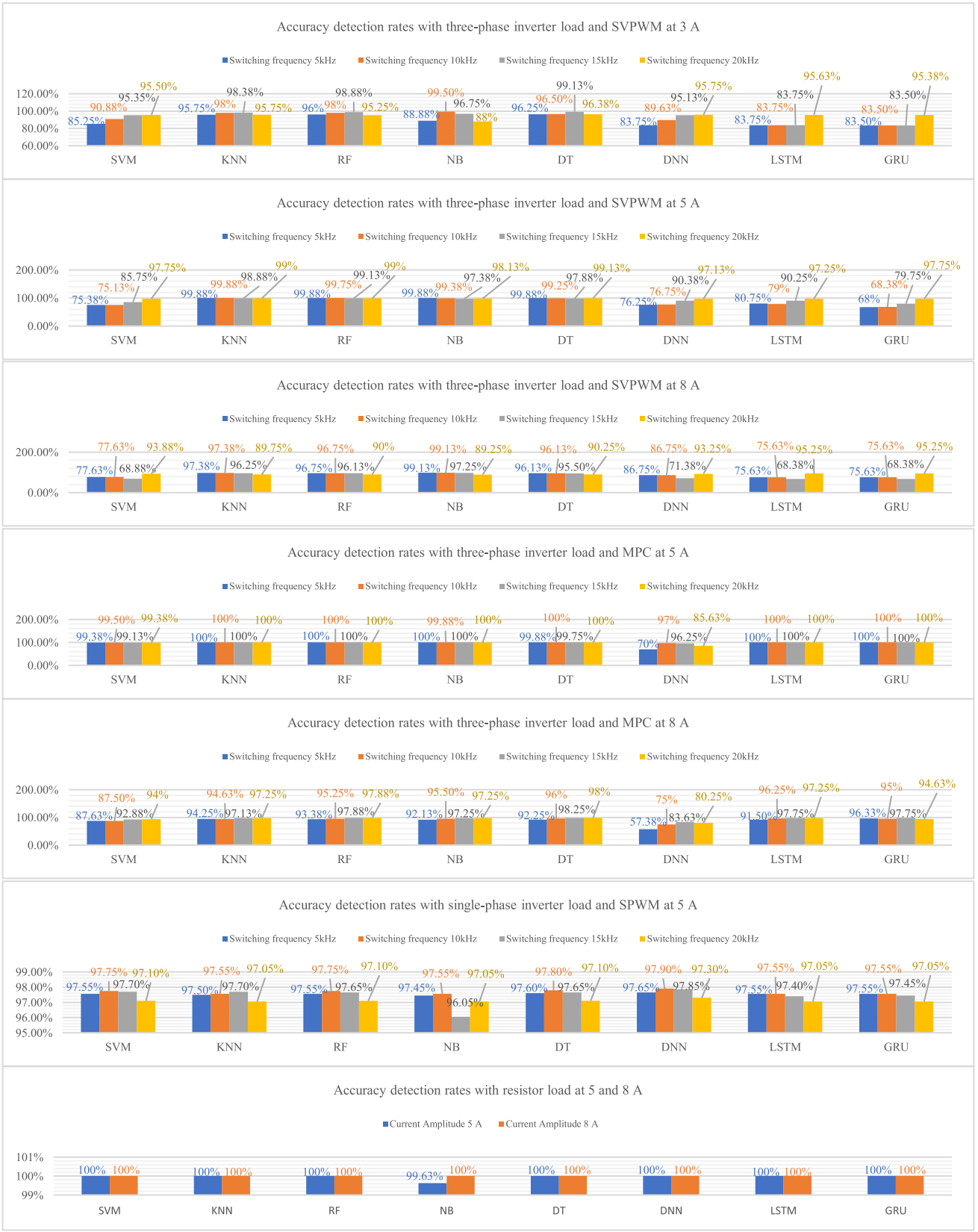

FIGURE 8. Accuracy detection rates for the enclosed type in different conditions.

performance and GRU had the lowest accuracy. In terms of the frequency range, the machine learning techniques' accuracy increased when the frequency increased from 5 to 15 kHz, and their highest accuracy was observed at 15 kHz. On the other hand, the deep learning techniques showed the highest accuracy at 20 kHz. When the current amplitude was 5 A, KNN, RF, NB, and DT showed the highest accuracy at 5 kHz and at 10, 15, and 20 kHz, KNN, RF, and DT showed the highest accuracies, respectively. GRU showed the lowest accuracy in the frequency ranges 5, 10, and 15 kHz, and DNN showed the lowest accuracy at 20 kHz. RF showed the best performance among the five machine learning techniques, whereas SVM had the lowest accuracy; however, the differences in the accuracies of KNN, RF, NB, and DT were fairly small. Among the three deep learning techniques, LSTM showed the best performance and GRU had the lowest accuracy. In terms of the frequency range, the accuracies of SVM and the three deep learning techniques increased with an increase in the frequency from 5 to 20 kHz. At 20 kHz, all AI algorithms showed similar and high performance. At current amplitude 8 A, NB showed the highest accuracy at 5, 10, and 15 kHz, and at 20 kHz, LSTM and GRU showed the highest accuracies. LSTM and GRU showed the lowest accuracies at 5, 10, and 15 kHz, and NB showed the lowest accuracy at 20 kHz. Among the five machine learning techniques, NB showed the best performance, and SVM had the lowest accuracy. Differences between the accuracies of KNN, RF, NB, and DT were significantly small. DNN showed the best performance at 5, 10, and 15 kHz among the three deep learning techniques, and LSTM and GRU had the best accuracy at 20 kHz. In terms of the frequency range, the accuracies of SVM and the three deep learning techniques increased and the accuracies of KNN, RF, NB, and DT decreased when the frequency increased from 5 to 20 kHz. In the case of a three-phase inverter load with MPC at 5 A, all techniques, except for DNN, showed high accuracy (above 99%) in all frequency ranges. SVM had the lowest accuracy; however, the accuracy difference between SVM and the other machine learning techniques was minimal. When the current amplitude was 8 A, GRU showed the highest accuracy at the switching frequency of 5 kHz, and at 10, 15, and 20 kHz, DT showed the highest accuracy. DNN showed the lowest accuracy in all frequency ranges. KNN, RF, NB, and LSTM also showed high performance (above 91%) in all frequency ranges. SVM showed mediocre performance compared with the other techniques at switching frequencies of 5 and 10 kHz. The accuracy of SVM, KNN, RF, and NB increased with the switching frequency from 5 to 20 kHz. On the other hand, the accuracies of DT, DNN, LSTM, and GRU increased with an increase in the switching frequency from 5 to 15 kHz but slightly decreased at 20 kHz. In the case of single-phase inverter load. The performance of all techniques was high (about 97%). DNN showed the best performance in all frequency ranges, and NB showed the lowest accuracy. However, the difference between the accuracies of all the techniques was minimal. When the resistor load was used. The performance of all techniques was high (almost 100%), and the arc fault could be detected correctly without miss or false detections, except for NB at 5 A.

Generally, data that are trained before testing are significantly beneficial for all AI techniques to achieve high performance for different current levels, load types, and switching frequencies. In the training process, the unique characteristics of each specific condition are learned, and they can subsequently be used to detect arc faults correctly.

B. UNENCLOSED TYPES

This section compares the detection rate regarding the input parameters and AI structures for the unenclosed types. As mentioned, this type was divided into two cases. Different data sets were trained and tested in each of the cases. Figure 9 shows dummy detection rates for the unenclosed type 1 when different DC current amplitudes and various loads were employed. In the case of three-phase inverter load with MPC, the dummy detection rates of the KNN, RF, and NB techniques were always lower than those of the three deep learning techniques at 5, 15, and 20 kHz. A similar trend was observed for KNN, RF, NB, and DT when the current amplitude was 8 A. In the case of single-phase inverter load, NB and LSTM showed the lowest rates, whereas SVM, KNN, RF, DT, and DNN reached the maximum rate (about 100%) at 5 A in all frequency ranges. All techniques showed the same performance for both 5 and 8 A current amplitudes when the resistor load was employed. In the case of three-phase inverter load with SVPWM, KNN, RF, LSTM, GRU showed high dummy detection rates at 4, 6, and 7 A current amplitudes in all frequency ranges. On the other hand, SVM, NB, and DT show the best detection rate except for NB at 6 A and DT at 4 A current amplitude. Figure 10 shows missing detection rates for the unenclosed type 1 when different DC current amplitudes and various loads were employed. In the case of three-phase inverter load with MPC, the performances of all techniques were similar at 5 A current amplitude in all frequency ranges. A similar trend was also observed for SVM, DNN, LSTM, GRU at 8 A current amplitude, whereas RF, NB, DT hit the maximum rate (100%) in all frequency ranges. In the case of single-phase inverter load, SVM, KNN, RF, DT, DNN, GRU showed the best rate, whereas NB and LSTM reached the maximum rate. When the resistor load was employed, all techniques reached the maximum rate for both 5 and 8 A current amplitudes except NB at 5 A. Three-phase inverter load with SVPWM, KNN, RF, LSTM, and GRU showed high performance in all frequency ranges. The other techniques showed mediocre performance and NB hit the maximum rate at 4 and 7 A current amplitudes.

Figure 11 shows accuracy detection rates for the unenclosed type 1 when different DC current amplitudes and various loads were employed. The accuracies of the KNN, RF, and NB algorithms were higher than those of the three deep learning algorithms at 5 A current amplitude and 5, 15, 20 kHz switching frequencies. At 5, 15, and 20 kHz,

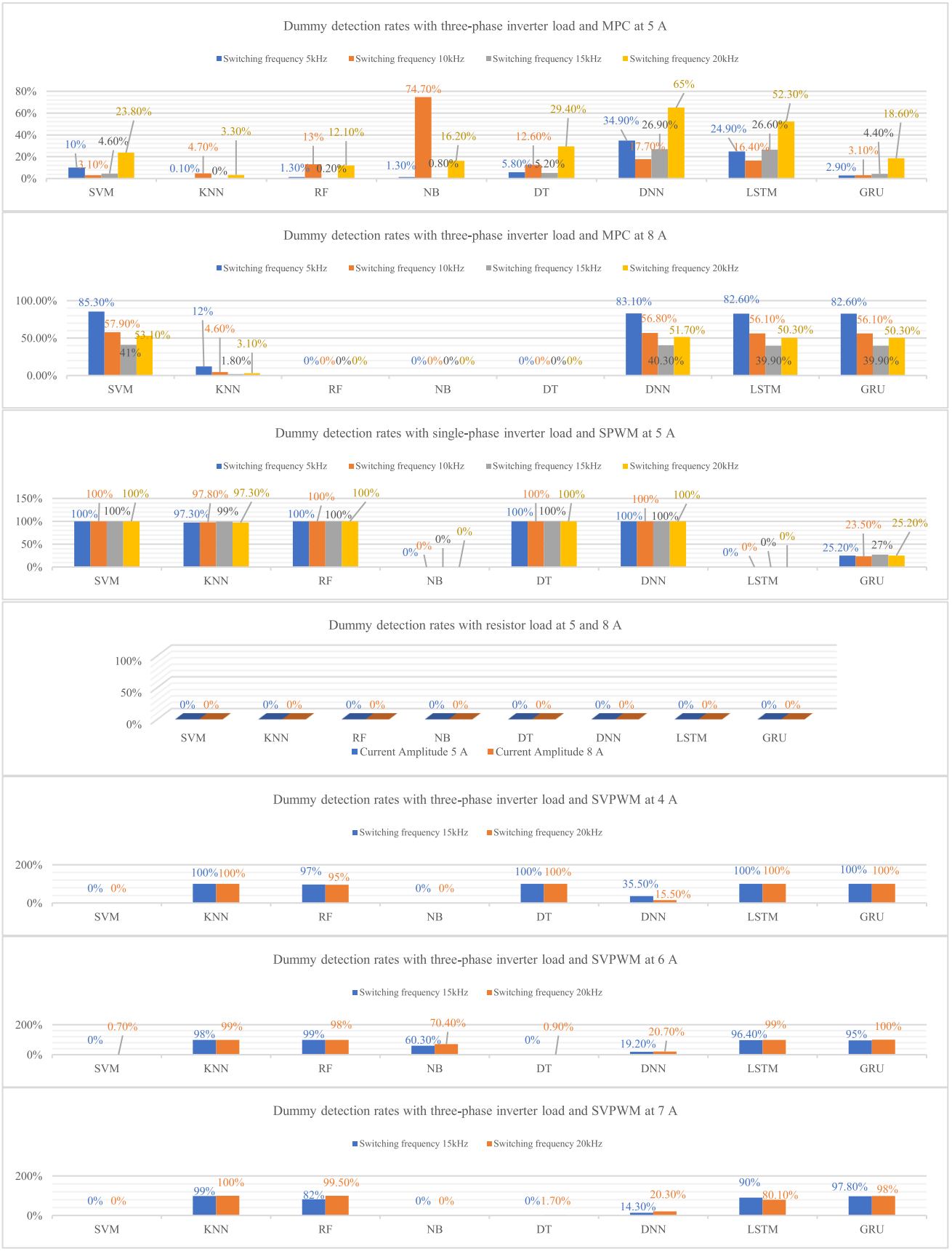

FIGURE 9. Dummy detection rates for the unenclosed type 1 in different conditions.

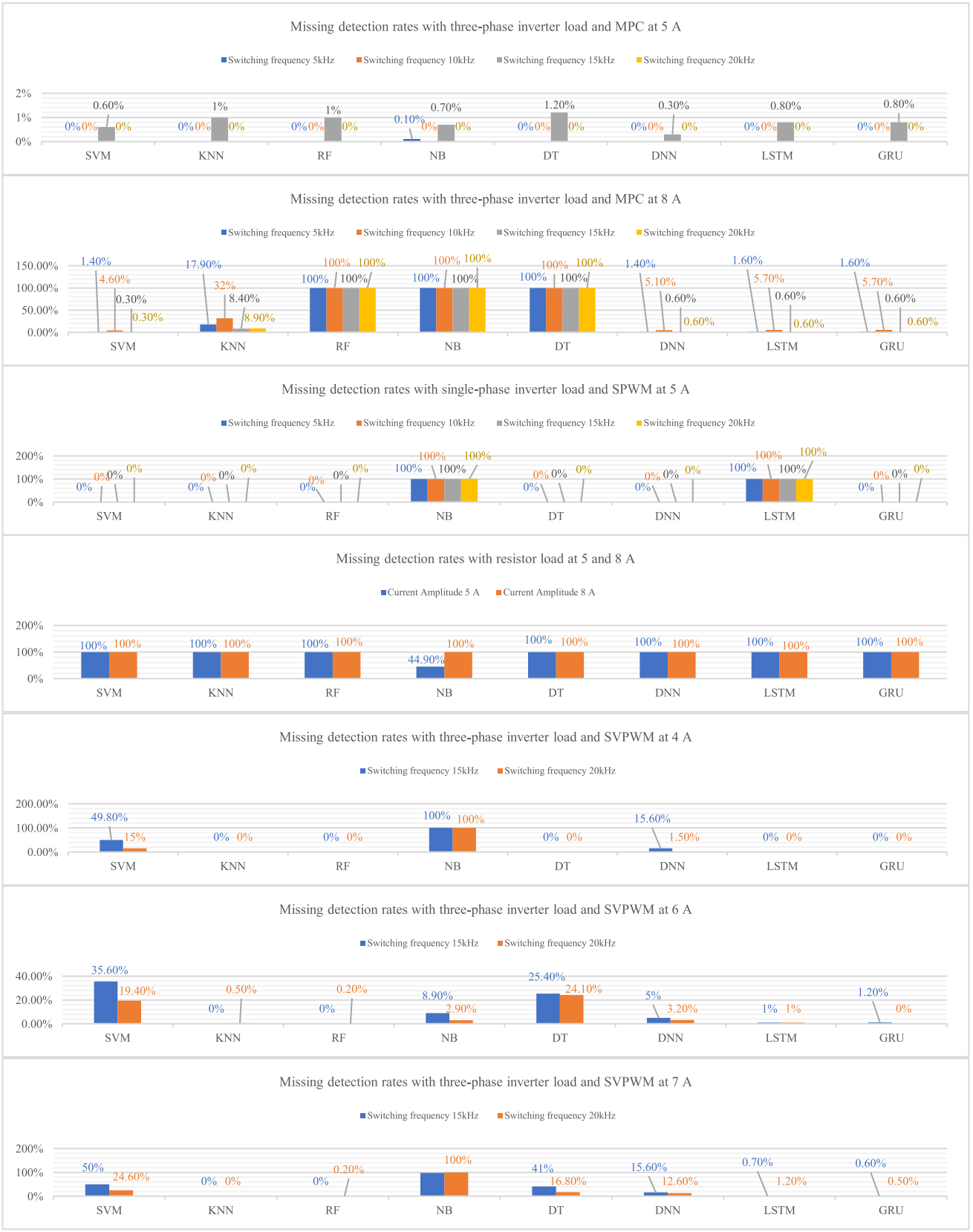

FIGURE 10. **Missing detection rates for the unenclosed type 1 in different conditions.**

FIGURE 11. Accuracy detection rates for the unenclosed type 1 in different conditions.

FIGURE 12. Dummy detection rates for the unenclosed type 2 in different conditions.

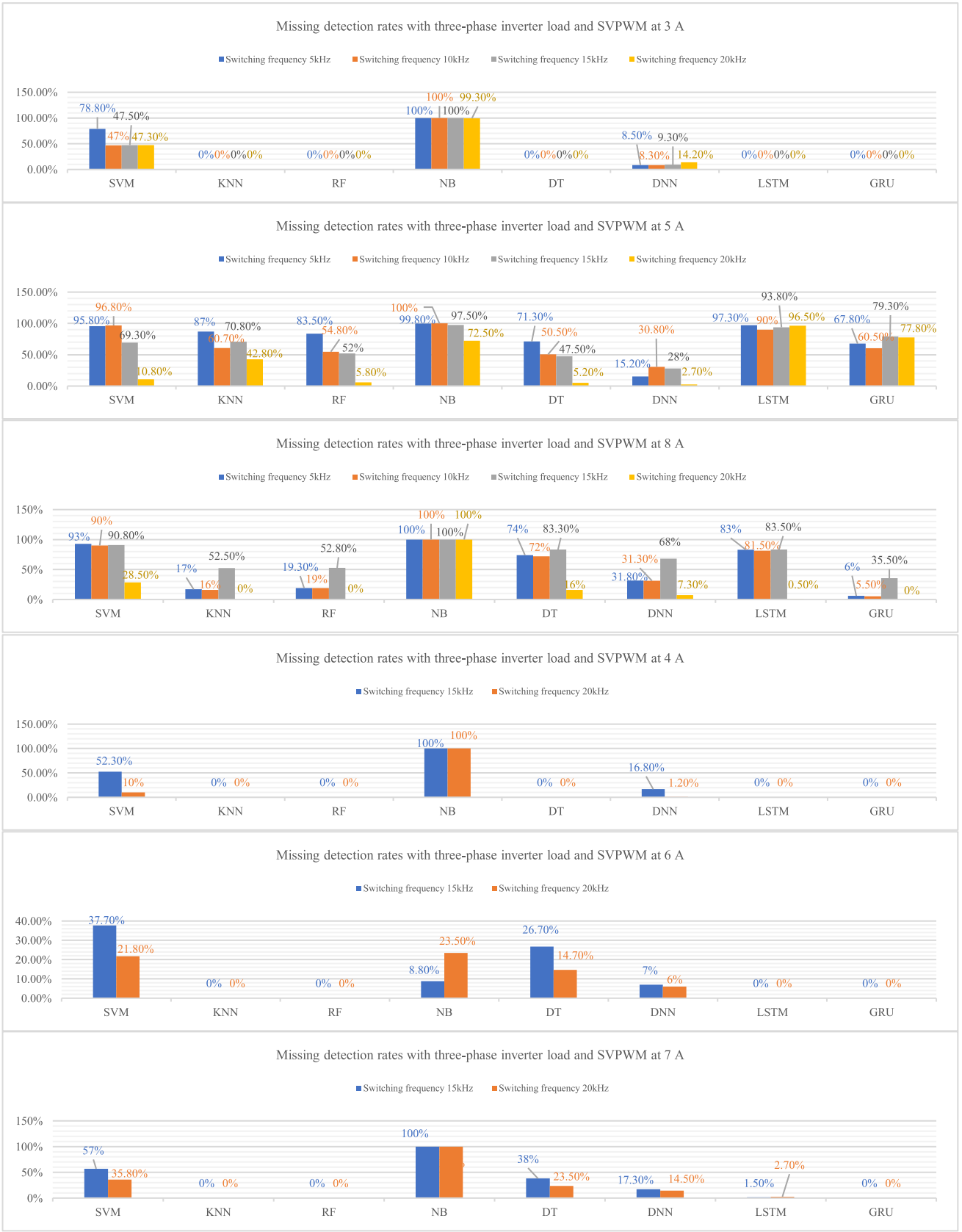

FIGURE 13. Missing detection rates for the unenclosed type 2 in different conditions.

FIGURE 14. **Accuracy detection rates for the unenclosed type 2 in different conditions.**

KNN showed the highest accuracy, and at 10 kHz, the SVM and GRU techniques showed the highest accuracies. At 5 and 20 kHz, DNN showed the lowest accuracy, and at 10 and 15 kHz, NB and LSTM showed the lowest accuracies, respectively. Among the five machine learning techniques, KNN showed the best performance. The difference between the accuracies of KNN, RF, and NB was significantly small at the frequency ranges of 5 and 15 kHz. Among the three deep learning techniques, GRU showed the best performance in all frequency ranges and DNN showed the lowest accuracy. In terms of the frequency range, the accuracies of all techniques decreased when the frequency increased from 5 to 20 kHz. When the current amplitude was 8 A. The KNN algorithm showed the highest accuracy in all frequency ranges, and RF, NB, and DT showed poor performance in all frequency ranges. The accuracy detection rates of SVM and the three deep learning techniques were similar to each other in all frequency ranges. Among the five machine learning techniques, KNN showed the best performance, and RF, NB, and DT had the lowest accuracy. Among the three deep learning techniques, LSTM and GRU showed the best performance in all frequency ranges. In terms of the frequency range, the accuracies of all techniques, except for RF, NB, and DT, increased from 5 to 15 kHz; the accuracies of RF, NB, and DT remained constant. The best performance of SVM, KNN, DNN, LSTM and GRU was observed at 15 kHz. In the case of single-phase inverter load, GRU showed the highest accuracy in all frequency ranges. However, at 10 kHz, the value of the highest accuracy was only 88.25%. This was almost 10% lower than the enclosed type. The other techniques showed poor performance in all frequency ranges. When the resistor load was employed, the performance of all techniques in both cases was poor, except for NB at 5 A. However, the accuracy of NB at 5 A was only 77.56%. It is surmised that the current characteristics of the resistor load were different from those of the single- and three-phase inverter loads. Thus, all learning models with inverter loads cannot detect the arc fault with high accuracy. In the case of three-phase inverter load with SVPWM, SVM showed the highest accuracy and DNN took second place at 4 A and the switching frequency of 15 kHz. By contrast, DNN had the highest accuracy and SVM took second place at the switching frequency of 20 kHz. The remaining algorithms showed poor performance at both 15 and 20 kHz. When the current amplitude was 6 A, at the switching frequency of 15 kHz, DNN showed the highest accuracy, and SVM showed the best performance at 20 kHz. The remaining algorithms, except for DT, showed poor performance at both 15 and 20 kHz. A similar trend at 7 A was observed for DNN and DT for 15 and 20 kHz switching frequency, respectively.

Figure 12 shows dummy detection rates for the unenclosed type 2 when different DC current amplitudes and three-phase inverter load with SVPWM were employed. SVM and NB showed the best rate, whereas KNN, RF, DT, LSTM, GRU hit the maximum rate at 3 A in all frequency ranges. When the current amplitudes were 5 and 8 A, all techniques showed high performances except DNN and KNN, RF, LSTM and GRU at 8 A current amplitude and 20 kHz switching frequency. When the current amplitudes were 4, 6, 7 A, the dummy detection rates of all techniques were similar that those in unenclosed type 1 with small differences. Figure 13 shows missing detection rates for the unenclosed type 1 when different DC current amplitudes and three-phase inverter load with SVPWM were employed. KNN, RF, DT, LSTM, GRU showed the best rate in all frequency ranges at 3 A current amplitude, whereas NB and SVM showed the highest and medium rates in all frequency ranges. When the current amplitude was 5 A, DNN showed the best performance, a similar trend was observed for KNN, RF and GRU at 8 A current amplitude. In contrast, the other techniques showed similar performance for both 5 and 8 A current amplitudes in all frequency ranges. When the current amplitudes were 4, 6, 7 A, all techniques' missing detection rates were similar to those in unenclosed type 1 with small differences.

Figure 14 shows accuracy detection rates for the unenclosed type 1 when different DC current amplitudes and three-phase inverter load were employed. At 3 A, DNN showed the highest accuracy at the switching frequencies of 5, 15, and 20 kHz, and SVM showed the best performance at the switching frequency of 10 kHz. Other AI techniques showed poor performance in all frequency ranges. When the DC current amplitude was 5 A, GRU showed the best performance at 5 kHz, and DNN showed the highest accuracy at 15 kHz. Furthermore, DT showed the highest accuracy at the switching frequencies of 10 and 20 kHz. The accuracy of the LSTM and GRU techniques fluctuated with an increase in the switching frequency, whereas the accuracy of the remaining techniques increased with the switching frequency. When the DC current amplitude was 8 A, GRU showed the highest accuracy at switching frequencies of 5, 10, and 15 kHz, and DNN exhibited the best performance at 20 kHz. NB showed the lowest accuracy in all switching frequency ranges. The accuracy of KNN, RF, and GRU decreased with an increase in the switching frequency, whereas that of SVM, DT, and LSTM increased with the switching frequency. When the DC current amplitudes were 4, 6, 7 A, the performances were similar to those in unenclosed type 1.

Clearly, the performance of all techniques for the enclosed type was generally higher than that for the unenclosed type. However, the poor performance for the unenclosed type showed that the load type and control technique could affect the accuracy of arc fault detection when the new data were not trained. Therefore, new data training is essential for a new load or new operation conditions for achieving high performance in DC series arc fault detection.

V. CONCLUSION

Using eight types of AI algorithms and various input parameters, combinations suitable for arc detection were examined. In the case of DC series arc enclosed type, KNN, RF, NB, and DT showed high performance in all switching frequency ranges. SVM, DNN, LSTM, and GRU showed mediocre

performance at low switching frequencies such as 5 and 10 kHz, they show high performance at high switching frequencies such as 15 and 20kHz. The difference in accuracies at high switching frequency is significantly slight between all AI techniques. Generally, the performance of all AI algorithms increases with the increase of frequency. The increase of frequency may increase the helpful information in each data set; thus, the accuracy can be improved.

In the case of DC series arc unenclosed type 1, the performance of all techniques is significantly degraded, especially the resistor load. It is guessed that the current characteristic of resistor load is different from the single- or three-phase inverter loads. Thus, all learning models of inverter loads cannot detect the arc fault with high accuracy. In the case of DC series arc unenclosed type 2, similarly to the unenclosed type 1, the performance of all AI techniques are low. In both unenclosed types 1 and 2, the performance of all techniques at high switching frequencies is higher than at low switching frequencies. The poor performances in the unenclosed type show that different load types or control techniques could affect the accuracy of arc fault detections without training the new data. Therefore, training new data when a new load or operation conditions is essential for achieving high performance in DC series arc fault detection.

The performances of machine learning techniques were better than deep learning techniques in low-frequency ranges. Deep learning techniques usually process raw data and do not require feature extraction to obtain high accuracy; some useful information might be lost during the feature extraction resulting in the poor performance of deep learning techniques. In addition, deep learning techniques consist of many neurons and layers, which can increase the computational cost and execution time. This could be useful for practical applications, which is a priority for cost and reliability.

Machine learning techniques showed high performance at low switching frequencies, small data sets, and simple implementation. However, their drawbacks are the need for feature extractions to maintain the high detection rates. On the other hand, deep learning techniques do not require any feature extraction to obtain high accuracy. They require a large data set and high computational cost due to their deeper structure than machine learning techniques. The depth and the width of layers in deep learning algorithms (DNN, LSTM, GRU) were chosen on the basis of the trial and error method. Many tests are required to find the most optimal performance. However, there is no way to guarantee that the chosen depths and widths yield the best performance. For example, the optimal depth and width of layers can be different if the trial number is different. Furthermore, the performance of deep learning algorithms varies with the operating conditions (current amplitude, load type, and load converter frequency). This means that the optimal depth and width of layers in one case are not optimal for other cases. As shown in the detection results, deep learning algorithms showed higher performance than the other AI techniques in several cases, whereas their performance was poor or mediocre in other cases.

It is interesting to note that no AI technique showed high performance in all test cases. Some techniques achieved high accuracies in specific conditions, otherwise, their accuracies were poor. It is recommended that for arc fault detection, several AI techniques should be combined to improve accuracy and maintain high performance in different operating conditions. Furthermore, all AI algorithms can be used to detect AC arc faults. However, the input features should be different from DC arc fault detection due to the difference in arc current characteristics, such as zero-crossing periods (flat shoulders) and high-frequency harmonic components. Several frequency domain analysis techniques such as fast Fourier transform, wavelet transform are helpful to extract features. This study offers a specific view on different learning techniques. This might be helpful research for selecting learning techniques, which can assist in building more robust and reliable systems when implementing an arc fault detection system regarding different priorities.

REFERENCES

[1] H. Xin, Z. Qu, J. Seuss, and A. Maknouninejad, "A self-organizing strategy for power flow control of photovoltaic generators in a distribution network," *IEEE Trans. Power Syst.*, vol. 26, no. 3, pp. 1462–1473, May 2011.

[2] M. Thomson and D. G. Infield, "Impact of widespread photovoltaics generation on distribution systems," *IET Renew. Power Gener.*, vol. 1, no. 1, pp. 33–40, Mar. 2007.

[3] B. Sahan, S. V. Araújo, C. Nöding, and P. Zacharias, "Comparative evaluation of three-phase current source inverters for grid interfacing of distributed and renewable energy systems," *IEEE Trans. Power Electron.*, vol. 26, no. 8, pp. 2304–2318, Aug. 2011.

[4] H. Qin, C. Wang, S. Liu, and Y. Liu, "Discussion on the technology of intelligent micro-grid and flexible distribution system," *Power Syst. Protection Control*, vol. 44, no. 20, pp. 17–23, Oct. 2016.

[5] R. H. Lee, "The other electrical hazard: Electric arc blast burns," *IEEE Trans. Ind. Appl.*, vol. IA-18, no. 3, pp. 246–251, May 1982.

[6] J. Yuventi, "DC electric arc-flash hazard-risk evaluations for photovoltaic systems," *IEEE Trans. Power Del.*, vol. 29, no. 1, pp. 161–167, Feb. 2014.

[7] W.-S. Moon, J.-C. Kim, A. Jo, S.-B. Bang, and W.-S. Ko, "Ignition characteristics of residential series arc fault in 220 V HIV wire," in *Proc. IEEE Ind. Appl. Soc. Annu. Meeting*, Vancouver, BC, Canada, Oct. 2014, pp. 1–5.

[8] S. Chen, X. Li, Z. Xie, and Y. Meng, "Time–frequency distribution characteristic and model simulation of photovoltaic series arc fault with power electronic equipment," *IEEE J. Photovolt.*, vol. 9, no. 4, pp. 1128–1137, Jul. 2019.

[9] G. Parise, L. Martirano, and M. Laurini, "Simplified arc-fault model: The reduction factor of the arc current," *IEEE Trans. Ind. Appl.*, vol. 49, no. 4, pp. 1703–1710, Jul. 2013.

[10] Q. Wang, B. W. Wang, H. L. Guan, and Z. Z. Zhao, "Model and experiment of low voltage AC series fault arc," in *Proc. CSU-EPSA*, vol. 30, pp. 26–35, Feb. 2018.

[11] J. Andrea, P. Besdel, O. Zirn, and M. Bournat, "The electric arc as a circuit component," in *Proc. 41st Annu. Conf. IEEE Ind. Electron. Soc. (IECON)*, Yokohama, Japan, Nov. 2015, pp. 003027–003034.

[12] F. M. Uriarte, A. L. Gattozzi, J. D. Herbst, H. B. Estes, T. J. Hotz, A. Kwasinski, and R. E. Hebner, "A DC arc model for series faults in low voltage microgrids," *IEEE Trans. Smart Grid*, vol. 3, no. 4, pp. 2063–2070, Dec. 2012.

[13] A. Khamkar and D. D. Patil, "Arc fault and flash signal analysis of DC distribution system sing artificial intelligence," in *Proc. Int. Conf. Renew. Energy Integr. Smart Grids, Multidisciplinary Approach Technol. Model. Simul. (ICREISG)*, Bhubaneswar, India, Feb. 2020, pp. 10–15.

[14] R. C. Zhang, J. H. Yang, and J. H. Du, "Study on in-process detection and diagnosis of faults arc based on early sounds signature and intermittent chaos," *Key Eng. Mater.*, vols. 381–382, pp. 611–614, Jun. 2008.

[15] C. J. Kim, "Electromagnetic radiation behavior of low-voltage arcing fault," *IEEE Trans. Power Del.*, vol. 24, no. 1, pp. 416–423, Jan. 2009.

[16] L. Zhu, J. Li, Y. Liu, and S. Ji, "Initial features of the unintended atmospheric pressure DC arcs and their application on the fault detection," *IEEE Trans. Plasma Sci.*, vol. 45, no. 4, pp. 742–748, Apr. 2017.
[17] K. Li, Z. Chen, Y. Z. Zhang, and Y. Wang, "Arc fault detection based on cluster analysis and electromagnetic radiation," *Electr. Mach. Control*, vol. 22, no. 163, pp. 98–105, May 2018.
[18] J. Jiang, M. Zhao, Z. Wen, C. Zhang, and R. Albarracín, "Detection of DC series arc in more electric aircraft power system based on optical spectrometry," *High Voltage*, vol. 5, no. 1, pp. 24–29, Feb. 2020.
[19] W. Yao, Z. Yanfeng, N. Feng, Z. Shuangle, and L. Kui, "Characterization and measurement method of DC arc electromagnetic radiation for photovoltaic systems," *Trans. China Electrotech. Soc.*, vol. 34, no. 14, pp. 2913–2921, Jul. 2019.
[20] J. Kim, S. Kwak, and S. Choi, "DC series arc detection algorithm based on adaptive moving average technique," *IEEE Access*, vol. 9, pp. 94426–94437, 2021.
[21] Q. Xiong, W. Chen, and S. Ji, "Review of research progress on characteristics, detection and localization approaches of fault arc in low voltage DC system," *Proc. CSEE*, vol. 40, no. 18, pp. 6015–6027, Sep. 2020.
[22] S. Tharmakulasingam, S. Lu, B. T. Phung, D. Zhang, and E. Ambikairajah, "Sustainable deep learning at grid edge for real-time high impedance fault detection," *IEEE Trans. Sustain. Comput.*, early access, Nov. 7, 2018, doi: 10.1109/TSUSC.2018.2879960.
[23] R. Liu, G. Meng, B. Yang, C. Sun, and X. Chen, "Dislocated time series convolutional neural architecture: An intelligent fault diagnosis approach for electric machine," *IEEE Trans. Ind. Inf.*, vol. 13, no. 3, pp. 1310–1320, Jun. 2017.
[24] T. de Bruin, K. Verbert, and R. Babuska, "Railway track circuit fault diagnosis using recurrent neural networks," *IEEE Trans. Neural Netw. Learn. Syst.*, vol. 28, no. 3, pp. 523–533, Mar. 2017.
[25] K. Xia, S. He, Y. Tan, Q. Jiang, J. Xu, and W. Yu, "Wavelet packet and support vector machine analysis of series DC ARC fault detection in photovoltaic system," *IEEJ Trans. Elect. Electron. Eng.*, vol. 14, no. 2, pp. 192–200, Feb. 2019.
[26] R. D. Telford, S. Galloway, B. Stephen, and I. Elders, "Diagnosis of series DC Arc faults—A machine learning approach," *IEEE Trans. Ind. Informat.*, vol. 13, no. 4, pp. 1598–1609, Aug. 2017.
[27] B. Grichting, J. Goette, and M. Jacomet, "Cascaded fuzzy logic based arc fault detection in photovoltaic applications," in *Proc. Int. Conf. Clean Elect. Power (ICCEP)*, Taormina, Italy, Jun. 2015, pp. 178–183.
[28] K. Yang, R. Zhang, J. Yang, C. Liu, S. Chen, and F. Zhang, "A novel arc fault detector for early detection of electrical fires," *Sensors*, vol. 16, no. 4, p. 500, 2016, doi: 10.3390/s16040500.
[29] H. Gao, X. Wang, T. Nguyen, F. Guo, Z. Wang, J. You, and Y. Deng, "Research on feature of series arc fault based on improved SVD," in *Proc. IEEE Holm Conf. Electr. Contacts*, Sep. 2017, pp. 325–331.
[30] Y. Wang, F. Zhang, and S. Zhang, "A new methodology for identifying arc fault by sparse representation and neural network," *IEEE Trans. Instrum. Meas.*, vol. 67, no. 11, pp. 2526–2537, Nov. 2018, doi: 10.1109/TIM.2018.2826878.
[31] S. Lu, T. Sirojan, B. T. Phung, D. Zhang, and E. Ambikairajah, "DA-DCGAN: An effective methodology for DC series arc fault diagnosis in photovoltaic systems," *IEEE Access*, vol. 7, pp. 45831–45840, 2019, doi: 10.1109/ACCESS.2019.2909267.
[32] S. Lu, A. Sahoo, R. Ma, and B. T. Phung, "DC series arc fault detection using machine learning in photovoltaic systems: Recent developments and challenges," in *Proc. 8th Int. Conf. Condition Monitor. Diagnosis (CMD)*, Oct. 2020, pp. 416–421, doi: 10.1109/CMD48350.2020.9287192.
[33] V. Le, X. Yao, C. Miller, and B.-H. Tsao, "Series DC arc fault detection based on ensemble machine learning," *IEEE Trans. Power Electron.*, vol. 35, no. 8, pp. 7826–7839, Aug. 2020, doi: 10.1109/TPEL.2020.2969561.
[34] *Outline of Investigation for Photovoltaic (PV) DC Arc-Fault Circuit Protection*, Standard UL 1699B, Underwriters Lab., Northbrook, IL, USA, 2013.
[35] J.-C. Kim and S.-S. Kwak, "Frequency-domain characteristics of series DC arcs in photovoltaic systems with voltage-source inverters," *Appl. Sci.*, vol. 10, no. 22, p. 8042, Nov. 2020.
[36] B. E. Boser, I. M. Guyon, and V. N. Vapnik, "A training algorithm for optimal margin classifiers," in *Proc. 5th Annu. workshop Comput. Learn. Theory (COLT)*, New York, NY, USA, 1992, pp. 144–152.
[37] T. Cover and P. Hart, "Nearest neighbor pattern classification," *IEEE Trans. Inf. Theory*, vol. IT-13, no. 1, pp. 21–27, Jan. 1967, doi: 10.1109/TIT.1967.1053964.
[38] L. Breiman, "Random forests," *Mach. Learn.*, vol. 45, no. 1, pp. 5–32, 2001.
[39] P. Langley, W. Iba, and K. Thompson, "An analysis of Bayesian classifiers," in *Proc. 10th Nat. Conf. Artif. Intell.*, 1992, pp. 223–228.
[40] L. Breiman, J. Friedman, R. Olshen, and C. Stone, *Classification and Regression Trees* (Statistics/Probability Series). Belmont, CA, USA: Wadsworth and Brooks, 1984.

HOANG-LONG DANG received the B.S. degree in electrical and electronics engineering from Ho Chi Minh University of Technology, Vietnam, in 2015. He is currently pursuing the combined M.S. and Ph.D. degree with the School of Electrical and Electronics Engineering, Chung-Ang University, Seoul, South Korea. His research interests include matrix converters, fault detections, and artificial intelligences.

JAECHANG KIM received the B.S. degree from the School of Electrical and Electronics Engineering, Chung-Ang University, Seoul, South Korea, in 2017, where he is currently pursuing the combined M.S. and Ph.D. degree with the School of Electrical and Electronics Engineering. His research interests include control and analysis for two-level, multilevel, and matrix converters.

SANGSHIN KWAK (Member, IEEE) received the Ph.D. degree in electrical engineering from Texas A&M University, College Station, TX, USA, in 2005. From 1999 to 2000, he was a Research Engineer at LG Electronics, Changwon, South Korea. From 2005 to 2007, he was a Senior Engineer at Samsung SDI Research and Development Center, Yongin, South Korea. From 2007 to 2010, he was an Assistant Professor with Daegu University, Gyeongsan, South Korea. Since 2010, he has been with Chung-Ang University, Seoul, South Korea, where he is currently a Professor. His current research interests include the design, modeling, control, and analysis of power converters for electric vehicles and renewable energy systems as well as the prognosis and fault tolerant control of power electronics systems.

SEUNGDEOG CHOI (Senior Member, IEEE) received the B.S. degree in electrical and computer engineering from Chung-Ang University, Seoul, South Korea, in 2004, the M.S. degree in electrical and computer engineering from Seoul National University, Seoul, in 2006, and the Ph.D. degree in electric power and power electronics from Texas A&M University, College Station, TX, USA, in 2010. From 2006 to 2007, he was a Research Engineer at LG Electronics, Seoul. From 2009 to 2012, he was a Research Engineer at Toshiba International Corporation, Houston, TX, USA. From 2012 to 2018, he was an Assistant Professor at The University of Akron, Akron, OH, USA. Since 2018, he has been working as an Associate Professor at Mississippi State University, Starkville, MS, USA. His current research interests include degradation modeling, fault tolerant control, and fault tolerant design of electric machines, power electronics, batteries, solar panels, and wider vehicular/aircraft microgrid systems.